

---

**Research article**

## Meshfree numerical approach for some time-space dependent order partial differential equations in porous media

**Abdul Samad<sup>1</sup>, Imran Siddique<sup>2</sup> and Zareen A. Khan<sup>3,\*</sup>**

<sup>1</sup> School of Mathematics, Northwest University, Xi'an 710127, China

<sup>2</sup> Department of Mathematics, University of Management and Technology, Lahore 54770, Pakistan

<sup>3</sup> Department of Mathematical Sciences, College of Sciences, Princess Nourah bint Abdulrahman University, P.O. Box 84428, Riyadh 11671, Saudi Arabia

\* **Correspondence:** Email: zakhan@pnu.edu.sa.

**Abstract:** In this article, the meshfree radial basis function method based on the Gaussian function is proposed for some time-space dependent fractional order partial differential equation (PDE) models. These PDE models have significant applications in chemical engineering and physical science. Some main advantages of the proposed method are that it is easy to implement, and the output response is quick and highly accurate, especially in the higher dimension. In this method, the time-dependent derivative terms are treated by Caputo fractional derivative while space-dependent derivative terms are treated by Riesz, Riemann-Liouville, and Grünwald-Letnikov derivatives. The proposed method is tested on some numerical examples and the accuracy is analyzed by  $\|L\|_\infty$ .

**Keywords:** advection-dispersion PDEs; Caputo derivatives; Grünwald-Letnikov derivatives; Riesz fractional derivatives; Riemann-Liouville fractional derivatives

**Mathematics Subject Classification:** 35G31, 35G35, 65D12

---

### 1. Introduction

The advection-dispersion equation has arisen in many chemical engineering and physical models [1]. In earth sciences, it is used as a solute transport water flow in surface and subsurface, stream, groundwater, ocean currents and deep river flows. Solute transport in streams, groundwater and rivers is controlled by heterogeneity or physical features in different levels. In the past, the advection-dispersion equation has been successfully used for mobile-immobile or transient storage models. In recent times, researchers highlighted the necessity of transport models from which heterogeneity and connectivity of spatial features inside solute transport can be described better. In porous media, the

transport flow is controlled by advection and dispersion equations which will predict a breakthrough curve [2].

The study of numerical models of solute transport is a basic aspect in parameter reconnaissance at both field and micro scales. The characterization of motion of solute transport is measured by the application of the advection-dispersion equation in porous media. However, there is some evidence that the advection-dispersion model failed to explain transport in heterogeneous, fractured and even in homogeneous media. The advection-dispersion and mobile immobile have fitted in breakthrough curves [3]. In both fractured and porous media, the results show that the mobile-immobile model is better than the advection-dispersion model, especially in explaining long tails and peaks of breakthrough curves. Because of such reasons, in tough-walled fracture, the mobile-immobile model is more effective than in smooth-walled fracture. The single-rate mobile-immobile model appears as the advection-dispersion model transport in the mobile region, whereas the transport in the immobile region by diffusion, making physical non-equilibrium [3–7].

Most scientific phenomena are formed through the fractional PDEs, which are either linear or nonlinear. PDEs with fractional orders are now becoming a useful study in the fields of physics, acoustics, engineering, chemistry, viscoelasticity, and biology [8–12].

For solute transport, the fractional mobile immobile advection-dispersion equation assumes power law waiting in the immobile region, yielding a fractional order in terms of time derivative. The fractional-order models are equipollent to non-fractional mobile-immobile transport with power law memory functions. There are some numerical methods used to study the mobile-immobile advection-dispersion model (see [13–17]). The advection-dispersion mobile-immobile model [13] is given by

$$r_1 w_\tau(v, \tau) + r_2 \mathbb{D}_\tau^{\zeta(v, \tau)} w(v, \tau) = r_3 \mathbb{D}_v^{\xi_1(v, \tau)} w(v, \tau) + r_4 \mathbb{D}_v^{\xi_2(v, \tau)} w(v, \tau) + R(v, \tau), \quad (1.1)$$

with the following initial and boundary conditions:

$$w(v, 0) = f(v), \quad v \in [a, b], \quad (1.2)$$

$$w(a, \tau) = f_1(\tau), \quad w(b, \tau) = f_2(\tau), \quad \tau \in [0, T], \quad (1.3)$$

where  $r_1$ ,  $r_2$ ,  $r_3$  and  $r_4$  are constants, and  $R(v, \tau)$  is known function. Also,  $0 < \zeta(v, \tau) \leq 1$ ,  $1 < \xi_1(v, \tau) \leq 2$  and  $0 < \xi_2(v, \tau) \leq 1$  are the time and space-dependent derivative orders of corresponding terms of Eq (1.1),  $\mathbb{D}_v^{\zeta(v, \tau)}$  w.r.t.  $v$  in domain  $D$ .

There are two types of numerical methods to deal with the PDE models. One is meshgrid method and the other one is meshfree method (see [18–23]). Currently, the meshfree methods are getting more attention of researchers to find numerical solutions to the PDEs, especially in fractional orders. Because meshfree methods do not require meshing, these methods only need uniform distributed nodes in the domain. The accuracy of meshfree methods is higher and less time-consuming than meshgrid methods. The homotopy analysis [24, 25], Variational iteration method [26], Spectral method [27], Adomian decomposition method [28, 29] and Radial basis function method [30, 31] are some well known meshfree methods.

In this research article, our focus is on the implementation of the radial basis function (RBF) method. Its implementation is easy in initial and boundary value problems and the choice of generating functions is also open. The meshfree radial basis function (RBF) method is used in both local and global forms. The RBF method is implemented through some generating functions such as

multiquadric, inverse multiquadric, inverse quadric and Gaussian. The main issue of these functions is the choice of shape parameter, which is an open choice and necessary for the best numerical results. This issue sometimes creates problems to find the numerical results, especially in higher dimensions. However, in Gaussian, the choice of shape parameter is not very challenging. The shape parameter  $c = \frac{1}{\sqrt{2}\sigma^2}$ , where  $\sigma$  is the variance between scattered data  $\{v_i, i = 1, 2, \dots, M\}$  and mean or center  $\bar{v}$  of the data (see [32]). Many researchers implemented RBF method on various PDE models. For example, Hosseini et al. [33] used RBF method to find the approximate solution of the fractional telegraph equation. Samad et al. [34] used RBF method to find the numerical solution of multi-term fractional-order PDEs. Similarly, Wang et al. [35, 36], Khan et al. [37], Ali et al. [38] and Nikan et al. [19, 20] have used meshfree RBF method to test the numerical results of various PDE models.

The current article covers the study of numerical solution of some time-space-dependent order PDE models using the Gaussian radial basis function (GA-RBF). The space derivatives are dealt with by Riesz fractional derivative and Grünwald-Letnikov derivative definitions. The time derivatives are iterated by the Caputo fractional derivative. The stability of the scheme is discussed in Section 3, whereas the numerical results are given in Section 4.

## 2. Materials and methods

### 2.1. Time derivatives

Let  $\delta\tau$  be the time interval for  $\tau \in [0, T]$ , then  $\tau_n = n\delta\tau$  for  $n = 0, 1, 2, \dots, N$ .

**Definition 2.1.** For any variable order  $\zeta(v, \tau)$ , the Coimbra operator  $\mathbb{D}$  is defined [39] by

$$\mathbb{D}_\tau^{\zeta(v, \tau)} w(v, \tau) = \frac{\int_{0_+}^\tau (\tau - \mu)^{-\zeta(v, \tau)} \frac{\partial w(v, \mu)}{\partial \mu} d\mu}{\Gamma(1 - \zeta(v, \tau))} + \frac{(w(v, \tau_{0_+}) - w(v, \tau_{0_-}))^{-\zeta(v, \tau)}}{\Gamma(1 - \zeta(v, \tau))},$$

where  $0 < \zeta(v, \tau) < 1$ . The Caputo fractional derivative can be expressed from Coimbra fractional derivative operator if  $w(v, \tau_{0_+}) = w(v, \tau_{0_-})$ , i.e.,

$$\mathbb{D}_\tau^{\zeta(v, \tau)} w(v, \tau) = \frac{1}{\Gamma(1 - \zeta(v, \tau))} \int_{0_+}^\tau (\tau - \mu)^{-\zeta(v, \tau)} \frac{\partial w(v, \mu)}{\partial \mu} d\mu.$$

Using finite difference method to discretize the time fractional term of Eq (1.1),

$$\begin{aligned} \mathbb{D}_\tau^{\zeta(v, \tau)} w(v, \tau_{n+1}) &= \frac{1}{\Gamma(1 - \zeta(v, \tau))} \int_0^{\tau_{n+1}} \frac{\partial w(v, \mu)}{\partial \mu} (\tau_{n+1} - \mu)^{-\zeta(v, \tau)} d\mu \\ &= \frac{1}{\Gamma(1 - \zeta(v, \tau))} \sum_{k=0}^n \int_{\tau_k}^{\tau_{k+1}} \frac{\partial w(v, \tau)}{\partial \mu} \frac{d\mu}{(\tau_{k+1} - \mu)^{\zeta(v, \tau)}} \\ &= \frac{1}{\Gamma(1 - \zeta(v, \tau))} \sum_{k=0}^n \frac{w(v, \tau_{k+1}) - w(v, \tau_k)}{\delta\tau} \int_{\tau_k}^{\tau_{k+1}} \frac{d\mu}{(\tau_{k+1} - \mu)^{\zeta(v, \tau)}} + \rho_{\delta\tau}^{k+1} \\ &= \frac{1}{\Gamma(1 - \zeta(v, \tau))} \sum_{k=0}^n \frac{w(v, \tau_{k+1}) - w(v, \tau_k)}{\delta\tau} \int_{\tau_{n-k}}^{\tau_{n+1-k}} \frac{d\varrho}{\varrho^{\zeta(v, \tau)}} + \rho_{\delta\tau}^{n+1} \\ &= \frac{1}{\Gamma(2 - \zeta(v, \tau))} \sum_{k=0}^n \frac{w(v, \tau_{n-k+1}) - w(v, \tau_{n-k})}{(\delta\tau)^{\zeta(v, \tau)}} [(k+1)^{1-\zeta(v, \tau)} - (k)^{1-\zeta(v, \tau)}] + \rho_{\delta\tau}^{n+1}. \end{aligned}$$

Thus, the time discretization for Eq (1.1) is

$$\begin{aligned} & r_1 w_\tau(\nu, \tau) + r_2 \mathbb{D}_\tau^{\zeta(\nu, \tau)} w(\nu, \tau) \\ &= \frac{r_1}{\delta\tau} (w^{n+1} - w^n) + \frac{r_2 \delta\tau^{-\zeta(\nu, \tau)}}{\Gamma(2 - \zeta(\nu, \tau))} (w^{n+1} - w^n) + \frac{r_2 \delta\tau^{-\zeta(\nu, \tau)}}{\Gamma(2 - \zeta(\nu, \tau))} \left( \sum_{k=1}^n \delta_k (w^{n+1-k} - w^{n-k}) \right), \end{aligned} \quad (2.1)$$

where  $\delta_k = (k+1)^{1-\zeta(\nu, \tau)} - k^{1-\zeta(\nu, \tau)}$  and the truncation error  $\rho_{\delta\tau}^{n+1}$  is bounded (see [34]).

**Lemma 2.1.**  $\delta_k = (k+1)^{1-\zeta(\nu, \tau)} - k^{1-\zeta(\nu, \tau)}$  has the following properties for  $k = 0, 1, 2, \dots$ .

(i)  $\delta_0 = 1, \delta_k > 0$ ,

(ii)  $\delta_k \geq \delta_{k+1}$ .

Let  $R_1 = \frac{r_1}{\delta\tau}$  and  $R_2 = \frac{r_2 \delta\tau^{-\zeta(\nu, \tau)}}{\Gamma(2 - \zeta(\nu, \tau))}$ , then Eq (2.1) is written as

$$r_1 w_\tau(\nu, \tau) + r_2 \mathbb{D}_\tau^{\zeta(\nu, \tau)} w(\nu, \tau) = (R_1 + R_2)[w^{n+1} - w^n] + R_2 \sum_{k=1}^n \delta_k (w^{n+1-k} - w^{n-k}). \quad (2.2)$$

## 2.2. Space discretization

### 2.2.1. RBF method

Let the solution of Eq (1.1) at  $n$ -time level be

$$w(\nu, \tau_n) = \sum_{m=1}^M \mu_m^n \varphi(r_m), \quad (2.3)$$

where  $r_m = \|\nu - \nu_m\|$ ,  $\nu_m$  are the centers of  $\nu$ , and  $\|\cdot\|$  is the Euclidean norm. Then, for the collocation points  $\{\nu_i : 1 \leq i \leq M\}$ , Eq (2.3) can be written as

$$w(\nu_i, \tau_n) = \sum_{m=1}^M \mu_m^n \varphi(r_{im}), \quad (2.4)$$

where  $r_{im} = \|\nu_i - \nu_m\|$ . The Gaussian function [32] for the proposed method is given by

$$\varphi(r_m) = \exp(-cr_m^2),$$

where  $c$  is the shape parameter. The value of the shape parameter can be adjusted [32] by the equation  $c = \frac{1}{\sqrt{2}\sigma^2}$ , where  $\sigma^2$  is the variance between  $\nu_i$  and the centers  $\nu_m$ . Thus, the matrix form of Eq (2.4) is obtained by

$$\begin{bmatrix} w(\nu_1, \tau_n) \\ w(\nu_2, \tau_n) \\ \vdots \\ w(\nu_M, \tau_n) \end{bmatrix} = \begin{bmatrix} \exp(-cr_{11}^2) & \exp(-cr_{12}^2) & \cdots & \exp(-cr_{1M}^2) \\ \exp(-cr_{21}^2) & \exp(-cr_{22}^2) & \cdots & \exp(-cr_{2M}^2) \\ \vdots & \vdots & \ddots & \vdots \\ \exp(-cr_{M1}^2) & \exp(-cr_{M2}^2) & \cdots & \exp(-cr_{MM}^2) \end{bmatrix} \times \begin{bmatrix} \mu_1^n \\ \mu_2^n \\ \vdots \\ \mu_M^n \end{bmatrix}. \quad (2.5)$$

Let  $A = \{\exp(-cr_{im}^2), 1 \leq i, m \leq M\}$ ,  $w^n = \{w(\nu_1, \tau_n), w(\nu_2, \tau_n), \dots, w(\nu_M, \tau_n)\}^T$  and  $\mu^n = \{\mu_1^n, \mu_2^n, \dots, \mu_M^n\}^T$ . Then, equation (2.5) is obtained by

$$w^n = A\mu^n. \quad (2.6)$$

Since  $A$  is invertible (see [33–36]),

$$\mu^n = A^{-1}w^n. \quad (2.7)$$

Also,  $A$  can be split into  $A_b$  and  $A_d$  such that  $A_b = \{\varphi(r_{im}), i = 1, M, 1 \leq m \leq M, 0 \text{ elsewhere}\}$  and  $A_d = \{\varphi(r_{im}), 2 \leq i \leq M-1, 1 \leq m \leq M, 0 \text{ elsewhere}\}$ .

### 2.2.2. Space derivatives

Applying  $\theta$ -weighted method to Eq (1.1) at time levels  $n$  and  $n+1$ ,

$$\begin{aligned} r_1 w_\tau(\nu, \tau_n) + r_2 \mathbb{D}_\tau^{\xi(\nu, \tau_n)} w(\nu, \tau_n) &= \theta \left( r_3 \mathbb{D}_\nu^{\xi_1(\nu, \tau_{n+1})} w(\nu, \tau_{n+1}) + r_4 \mathbb{D}_\nu^{\xi_2(\nu, \tau_{n+1})} w(\nu, \tau_{n+1}) \right) \\ &\quad + (1 - \theta) \left( r_3 \mathbb{D}_\nu^{\xi_1(\nu, \tau_n)} w(\nu, \tau_n) + r_4 \mathbb{D}_\nu^{\xi_2(\nu, \tau_n)} w(\nu, \tau_n) \right) + R(\nu, \tau_{n+1}), \end{aligned} \quad (2.8)$$

where  $0 \leq \theta \leq 1$ .

**Lemma 2.2.** If  $w(\nu, \tau) \in L_1(\Omega)$  and  $\mathbb{D}_\nu^{\xi(\nu, \tau)} w(\nu, \tau) \in C(\Omega)$ , where  $0 \leq p-1 < \xi(\nu, \tau) < p$ , then the normalized Grünwald-Letnikov approximation is obtained by

$${}_a \mathbb{D}_\nu^{\xi(\nu_i, \tau_n)} w(\nu_i, \tau_n) = (\delta\nu)^{-\xi(\nu_i, \tau_n)} \sum_{j=0}^{i-1} \psi_j(\xi(\nu_i, \tau_n)) w(\nu_{i-j}, \tau_n) + O(\delta\nu), \quad (2.9)$$

$${}_b \mathbb{D}_\nu^{\xi(\nu_i, \tau_n)} w(\nu_i, \tau_n) = (\delta\nu)^{-\xi(\nu_i, \tau_n)} \sum_{j=0}^{M-i} \psi_j(\xi(\nu_i, \tau_n)) w(\nu_{i+j}, \tau_n) + O(\delta\nu), \quad (2.10)$$

where  $\psi_j(\xi(\nu_i, \tau_n)) = \frac{\Gamma(j-\xi(\nu_i, \tau_n))}{\Gamma(j+1)\Gamma(-\xi(\nu_i, \tau_n))}$ ,  $i = 1, 2, \dots, M$  are the number of collocation nodes,  $j = 0, 1, 2, \dots$ .

**Lemma 2.3.** For  $1 \leq i \leq M$ ,  $0 \leq n \leq N$ , the coefficients  $\psi_j(\xi_i^n)$  satisfy the following properties for  $1 < \xi(\nu, \tau) \leq 2$ .

- (i)  $\psi_0(\xi_i^n) = 1$ ,  $\psi_1(\xi_i^n) < 0$ ,
- (ii)  $\psi_j(\xi_i^n) > 0$  for  $j \geq 2$ ,
- (iii)  $\sum_{j=0}^{\infty} \psi_j(\xi_i^n) = 0$ ,  $\sum_{j=0}^{\lambda} \psi_j(\xi_i^n) < 0$  for  $\lambda \geq 1$ .

*Proof.* Since for  $j \geq 0$ ,  $\psi_j(\xi_i^n) = \frac{\Gamma(j-\xi_i^n)}{\Gamma(j+1)\Gamma(-\xi_i^n)}$ , it is easy to verify (i) by putting  $j = 0, 1$ . Also,

$$\psi_{j+1}(\xi_i^n) = \frac{\Gamma(j+1-\xi_i^n)}{\Gamma(j+2)\Gamma(-\xi_i^n)} = \frac{(j-\xi_i^n)}{(j+1)} \frac{\Gamma(j-\xi_i^n)}{\Gamma(j+1)\Gamma(-\xi_i^n)} = \frac{j-\xi_i^n}{j+1} \psi_j(\xi_i^n),$$

for  $1 < \xi_i^n \leq 2$  it is clear from above that  $\psi_j(\xi_i^n) > 0$  for  $j \geq 0$ . Hence, (ii) is satisfied. Also, consider  $(1-y)^{\xi_i^n} = \sum_{j=0}^{\infty} \psi_j(\xi_i^n) y^j$  and let  $y = 1$ , we obtain  $\sum_{j=0}^{\infty} \psi_j(\xi_i^n) = 0$ . Further,  $\sum_{j=0}^{\lambda} \psi_j(\xi_i^n) < 0$  for  $\lambda \geq 1$ .

**Lemma 2.4.** For  $0 < \xi(\nu, \tau) \leq 1$ , the coefficients  $\{\psi_j(\xi_i^n), 1 \leq i \leq M, 0 \leq n \leq N\}$  satisfy the following properties:

- 
- (i)  $\psi_0(\xi_i^n) = 1$ ,  $\psi_j(\xi_i^n) < 0$  for  $j \geq 1$ ,  
(ii)  $\sum_{j=0}^{\infty} \psi_j(\xi_i^n) = 0$ ,  $\sum_{j=0}^{\lambda} \psi_j(\xi_i^n) > 0$  for  $\lambda \geq 1$ .

*Proof.* Similar to Lemma 2.3.

Now, from Eqs (2.9) and (2.10), and according to the Riesz fractional derivative operator [40], we have

$$\mathbb{D}_v^{\xi(v_i, \tau_n)} w(v_i, \tau_n) = C_{\xi(v_i, \tau_n)} \left( {}_a \mathbb{D}_v^{\xi(v_i, \tau_n)} + {}_b \mathbb{D}_v^{\xi(v_i, \tau_n)} \right) w(v_i, \tau_n),$$

where  $C_{\xi(v_i, \tau_n)} = \frac{1}{-2 \cos \frac{\pi \xi(v_i, \tau_n)}{2}}$ . For  $i = 1, 2, \dots, M$  and  $m = j + 1$ , using Eq (2.9), we have

$${}_a \mathbb{D}_v^{\xi(v_i, \tau_n)} w(v_i, \tau_n) = (h_i^n * G^n(i, m)) w(v_i, \tau_n), \quad (2.11)$$

and from Eq (2.10),

$${}_b \mathbb{D}_v^{\xi(v_i, \tau_n)} w(v_i, \tau_n) = (h_i^n * G_T^n(i, m)) w(v_i, \tau_n), \quad (2.12)$$

where '\*' shows the product of the  $i$ -th component of  $h_i$  with corresponding row of either  $G(i, m)$  or  $G_T(i, m)$  at  $n$  time level.  $h_i^n = C_{\xi(v_i, \tau_n)} * (\delta v)^{-\xi(v_i, \tau_n)}$ .

$$G(i, m) = \begin{cases} 0, & \text{for } i < m, \\ 1, & \text{for } i = m, \\ \frac{\Gamma(i-m+1-\xi(v_i, \tau_n))}{\Gamma(i-m+2)\Gamma(-\xi(v_i, \tau_n))}, & \text{for } i > m, \end{cases}$$

and  $G_T$  is the transpose of order  $M$  matrix  $G$ . Thus,

$$\mathbb{D}_v^{\xi(v_i, \tau_n)} w(v_i, \tau_n) = h_i^n * (G + G_T) w_i^n. \quad (2.13)$$

Now, using Eq (2.13), we obtain from Eq (2.8) as

$$\begin{aligned} & r_1 w_\tau(v, \tau_n) + r_2 \mathbb{D}_\tau^{\zeta(v, \tau_n)} w(v, \tau_n) \\ &= \theta \left( r_3 h(\xi_1^{n+1}) * (G_{\xi_1^{n+1}} + G_{\xi_1^{n+1} T}) w^{n+1} + r_4 h(\xi_2^{n+1}) * (G_{\xi_2^{n+1}} + G_{\xi_2^{n+1} T}) w^{n+1} \right) \\ & \quad + (1 - \theta) \left( r_3 h(\xi_1^n) * (G_{\xi_1^n} + G_{\xi_1^n T}) w^n + r_4 h(\xi_2^n) * (G_{\xi_2^n} + G_{\xi_2^n T}) w^n \right) + R^{n+1} + O(\delta v). \end{aligned} \quad (2.14)$$

Let  $W_1^n = G_{\xi_1^n} + G_{\xi_1^n T}$  and  $W_2^n = G_{\xi_2^n} + G_{\xi_2^n T}$ , Eq (2.14) becomes

$$\begin{aligned} & r_1 w_\tau(v, \tau_n) + r_2 \mathbb{D}_\tau^{\zeta(v, \tau_n)} w(v, \tau_n) \\ &= \theta \left( r_3 h(\xi_1^{n+1}) * W_1^{n+1} w^{n+1} + r_4 h(\xi_2^{n+1}) * W_2^{n+1} w^{n+1} \right) \\ & \quad + (1 - \theta) \left( r_3 h(\xi_1^n) * W_1^n w^n + r_4 h(\xi_2^n) * W_2^n w^n \right) + R^{n+1} + O(\delta v). \end{aligned} \quad (2.15)$$

### 2.3. Numerical scheme

Comparing Eq (2.2) with Eq (2.15), we obtain

$$\begin{aligned} & (R_1 + R_2)[w^{n+1} - w^n] + R_2 \sum_{k=1}^n \delta_k (w^{n+1-k} - w^{n-k}) \\ &= \theta \left( r_3 h(\xi_1^{n+1}) * W_1^{n+1} w^{n+1} + r_4 h(\xi_2^{n+1}) * W_2^{n+1} w^{n+1} \right) \\ & \quad + (1 - \theta) \left( r_3 h(\xi_1^n) * W_1^n w^n + r_4 h(\xi_2^n) * W_2^n w^n \right) + R^{n+1} + O(\delta v). \end{aligned} \quad (2.16)$$

After equation of the terms at  $n$  and  $n + 1$  time levels and using Eq (2.6), we obtain

$$\begin{aligned} & (R_1 + R_2)A\mu^{n+1} - \theta(r_3h(\xi_1^{n+1}) * W_1^{n+1}A\mu^{n+1} + r_4h(\xi_2^{n+1}) * W_2^{n+1}A\mu^{n+1}) \\ &= (R_1 + R_2)A\mu^n + (1 - \theta) \times (r_3h(\xi_1^n) * W_1^nA\mu^n + r_4h(\xi_2^n) * W_2^nA\mu^n) \\ &\quad - R_2 \sum_{k=1}^n \delta_k(w^{n+1-k} - w^{n-k}) + R^{n+1} + F^{n+1}. \end{aligned} \quad (2.17)$$

Thus,

$$P\mu^{n+1} = Q\mu^n - R_2 \sum_{k=1}^n \delta_k(w^{n+1-k} - w^{n-k}) + R^{n+1} + F^{n+1}, \quad (2.18)$$

where

$$\begin{aligned} P &= (R_1 + R_2)A - \theta[r_3h(\xi_1^{n+1}) * W_1^{n+1}A + r_4h(\xi_2^{n+1}) * W_2^{n+1}A], \\ Q &= (R_1 + R_2)A + (1 - \theta)[r_3h(\xi_1^n) * W_1^nA + r_4h(\xi_2^n) * W_2^nA], \\ F^{n+1} &= [f_1(a, \tau^{n+1}), 0, \dots, 0, f_2(b, \tau^{n+1})]_T. \end{aligned}$$

Let

$$\Phi^{n+1} = R^{n+1} + F^{n+1} - R_2 \sum_{k=1}^n \delta_k(w^{n+1-k} - w^{n-k}),$$

then

$$\mu^{n+1} = P^{-1}Q\mu^n + P^{-1}\Phi^{n+1}. \quad (2.19)$$

Again using Eqs (2.6) and (2.7), Eq (2.19) can be written as

$$w^{n+1} = AP^{-1}QA^{-1}w^n + AP^{-1}\Phi^{n+1}. \quad (2.20)$$

Thus, Eq (2.20) is the required numerical scheme.

### 3. Stability and convergence

The developed scheme for Eq (1.1) is the recurrence relation  $w(\tau_n)$  and  $w(\tau_{n+1})$  for  $n = 0, 1, 2, \dots, N$ . The elements of the amplification matrix  $\mathbb{F} = AP^{-1}QA^{-1}$  are dependent on the constant number  $c_i = \frac{\delta\tau^\zeta}{(\delta\nu)^{(\xi_1, \xi_2)}}$ , where  $\zeta$  is the time order and  $\xi_1, \xi_2$  are space order differential operators respectively.  $\delta\tau$  is the time step size and  $\delta\nu$  is spatial step size at successive nodes. Now let us consider the exact solution of Eq (1.1) be  $\mathcal{W}^n$  at  $\tau^n$ .

There are some important theorems from G. E. Fasshauer [32], whose statements are given below.

#### Theorem 3.1.

$$\left| D^\alpha g(\nu) - D^\alpha P_g(\nu) \right| \leq C \delta\nu_{\chi, \Omega}^{k-|\alpha|} \sqrt{\mathbb{C}_\Theta(x)} |g_{\mathbf{x}_\phi}|,$$

provided that  $\delta\nu_{\chi, \Omega} \leq \delta\nu_0$ , where

$$\mathbb{C}_\Theta(\nu) = \max_{\substack{\alpha_1, \alpha_2 \in \mathbb{N}_0^s \\ |\alpha_1| + |\alpha_2| = 2k}} \max_{w, \nu \in \Omega \cap B(x, c_2 \delta\nu_\chi, \Omega)} \left| D^{\alpha_1} D^{\alpha_2} \Theta(w, \nu) \right|.$$

**Theorem 3.2.** Let  $\Gamma \subseteq \mathcal{R}^s$  be open and bounded which satisfies the interior cone condition, and let  $\Theta \in C^{2k}(\Gamma \times \Gamma)$  be symmetric and strictly conditionally positive definite of order  $n$  on  $\mathcal{R}^s$ . Assign the interpolant to  $g \in \mathbf{N}_\phi(\Gamma)$  on the  $(n - 1)$  unisolvant set  $\chi$  by  $P_g$ . Fix  $\gamma \in \mathbb{N}_0^s$  taking  $|\alpha| \leq k$ . Then, there exist positive constants  $\delta\nu_0$  and  $C$  (independent of  $\nu$ ,  $g$  and  $\Theta$ ) such that

$$|D^\alpha g(\nu) - D^\alpha P_g(\nu)| \leq C_k(\delta\nu)^{k-|\alpha|} |w_{\mathbf{N}_\phi(\Gamma)}|,$$

where  $\mathbf{N}_\phi(\Gamma)$  represents the native space of RBF and  $g \in \mathbf{N}_\phi(\Gamma)$ . Since the Gaussian is an infinitely smooth function, application of the above theorem yields high algebraic convergence rates. So it is concluded that for every  $k \in \mathbb{N}$  and  $|\alpha| \leq k$ , we have

$$|D^\alpha \mathcal{W}(\nu) - D^\alpha w(\nu)| \leq C_k(\delta\nu)^{k-|\alpha|} |u_{\mathbf{N}_\phi(\Gamma)}|,$$

where  $\mathcal{W}$  and  $w$  are the respective exact and numerical solutions. Let us assume that Eq (2.20) is accurate with respect to space orders  $1 < \xi_1 \leq 2$  and  $0 < \xi_2 \leq 1$ , then

$$w^{n+1} = \mathcal{R}w^n + AP^{-1}\Phi^{n+1} + O(\delta\tau^{2-\zeta} + \delta\nu^{\xi_1,\xi_2}), \quad \delta\tau, \delta\nu \rightarrow 0. \quad (3.1)$$

Let us define the residual by  $e^p = \mathcal{W}^p - w^p$ , then

$$e^{n+1} = \mathcal{R}e^n + O(\delta\tau^{2-\zeta} + \delta\nu^{\xi_1,\xi_2}), \quad \delta\tau, \delta\nu \rightarrow 0. \quad (3.2)$$

Now, by Lax-Richtmyer definition of stability [18], the numerical model (2.20) is stable if

$$\|\mathcal{R}\| \leq 1. \quad (3.3)$$

If  $\mathcal{R}$  is normal, then  $\|\mathcal{R}\| = \rho(\mathcal{R})$ ; otherwise,  $\rho(\mathcal{R}) \leq \|\mathcal{R}\|$  is always satisfied. Let us assume that  $\delta\nu$  and  $\delta\tau$  are small enough such that the constant  $c = \frac{\delta\tau^\zeta}{\delta\nu^{\xi_1,\xi_2}}$ . Therefore, there exists a constant  $\varphi$  such that

$$\|e^{n+1}\| \leq \|\mathcal{R}\| \cdot \|e^n\| + \varphi(\delta\tau^\zeta + \delta\nu^{\xi_1,\xi_2}), \quad n \geq 0. \quad (3.4)$$

Now,  $e^0 = 0$ , as  $e^n$  satisfies the initial condition and boundary condition. Thus, using mathematical induction, we obtain from Eq (3.4)

$$\|e^{n+1}\| \leq (1 + \|\mathcal{R}\| + \|\mathcal{R}\|^2 + \cdots + \|\mathcal{R}\|^n)\varphi(\delta\tau^\zeta + \delta\nu^{\xi_1,\xi_2}), \quad n \geq 0. \quad (3.5)$$

Using geometric series property, we obtain

$$\|e^{n+1}\| \leq (n + 1)\varphi(\delta\tau^\zeta + \delta\nu^{\xi_1,\xi_2}), \quad n \geq 0. \quad (3.6)$$

Thus, the numerical model given in Eq (2.20) is convergent.

#### 4. Numerical results and discussion

In this part, the numerical results are discussed for numerical model (Eq (2.19)) obtained from Eq (1.1) along with initial and boundary conditions. The accuracy of all examples is analyzed by the following equations:

$$\|L\| = |\mathcal{W}^n - w^n|, \quad \|L\|_\infty = \max(\|L\|), \quad (4.1)$$

where  $\mathcal{W}$  and  $w$  are the exact and numerical solutions. The space and time convergence rates are measured by the following formulae:

$$\frac{\log_{10}(e_{\delta\nu_k}/e_{\delta\nu_{k+1}})}{\log_{10}(\delta\nu_k/\delta\nu_{k+1})} \text{ and } \frac{\log_{10}(e_{\delta\tau_k}/e_{\delta\tau_{k+1}})}{\log_{10}(\delta\tau_k/\delta\tau_{k+1})}.$$

**Example 4.1.** Set  $r_1 = r_2 = r_3 = 1$  and  $r_4 = -1$  in Eq (1.1) and consider  $\zeta(v, \tau) = 1 - 0.5e^{-v\tau}$ ,  $\xi_1(v, \tau) = 1.7 + 0.5e^{-\frac{v^2}{1000} - \frac{\tau}{50} - 1}$  and  $\xi_2(v, \tau) = 0.7 + 0.5e^{-\frac{v^2}{1000} - \frac{\tau}{50} - 1}$ , where  $(v, \tau) = [0, 1] \times [0, 1]$ . The initial and boundary conditions are

$$w(v, 0) = 0, \quad w(0, \tau) = 0 = w(1, \tau),$$

$$R(v, \tau) = \mathcal{R}_1(v, \tau) - \mathcal{R}_2(v, \tau) + \mathcal{R}_3(v, \tau),$$

where  $\mathcal{R}_1(v, \tau) = v(1-v)\left(2\tau + \frac{2\tau^{1-\zeta(v,\tau)}}{\Gamma(3-\zeta(v,\tau))}\right)$ ,  $\mathcal{R}_2(v, \tau) = \tau^2\left(\frac{v^{1-\xi_1(v,\tau)}}{\Gamma(2-\xi_1(v,\tau))} - \frac{2v^{2-\xi_1(v,\tau)}}{\Gamma(3-\xi_1(v,\tau))}\right)$ ,  $\mathcal{R}_3(v, \tau) = \tau^2\left(\frac{v^{1-\xi_2(v,\tau)}}{\Gamma(2-\xi_2(v,\tau))} - \frac{2v^{2-\xi_2(v,\tau)}}{\Gamma(3-\xi_2(v,\tau))}\right)$ ,  $\mathcal{W}(v, \tau) = \tau^2v(1-v)$  is the exact solution. The numerical results vs exact solutions along with errors are shown in Table 1. The computed  $\max(\|L\|)$  values are shown in Table 2 along with time and space convergence. The results are also shown in Figures 1–3. In Figure 1,  $\delta\nu = 0.001$  and  $\delta\tau = 0.001$  for 3D surface plot, while  $\delta\nu = 0.1$  and  $\delta\tau = 0.1$  for plot3 graph. In Figure 2, the error graphs are shown on 3D surfaces at  $N = 50, 500, 1000$  and  $\delta\tau = 0.001$  where  $\tau = 1$  while Figure 3 shows convergence rates w.r.t. space and time respectively.

**Example 4.2.** Put  $r_1 = r_2 = 1$ ,  $r_3 = 3$  and  $r_4 = -2$  and consider  $\zeta(v, \tau) = 0.75 - 0.5e^{v\tau}$ ,  $\xi_1(v, \tau) = 1.55 + 0.35 \cos(\pi v\tau)$  and  $\xi_2(v, \tau) = 0.65 + 0.25 \sin(\pi v\tau)$ , where  $(v, \tau) = [0, 1] \times [0, 1]$ .

The initial and boundary conditions are

$$w(v, 0) = 0,$$

$$w(0, \tau) = 0 = w(L, \tau), \quad R(v, \tau) = \mathcal{R}_1(v, \tau) - 3\mathcal{R}_2(v, \tau) + 2\mathcal{R}_3(v, \tau),$$

where  $\mathcal{R}_1(v, \tau) = v^2(1-v)\left(1 + \frac{\tau^{1-\zeta(v,\tau)}}{\Gamma(2-\zeta(v,\tau))}\right)$ ,  $\mathcal{R}_2(v, \tau) = \left(\frac{2v^{2-\xi_1(v,\tau)}}{\Gamma(3-\xi_1(v,\tau))} - \frac{6v^{3-\xi_1(v,\tau)}}{\Gamma(4-\xi_1(v,\tau))}\right)\tau$ ,  $\mathcal{R}_3(v, \tau) = \left(\frac{2v^{2-\xi_2(v,\tau)}}{\Gamma(3-\xi_2(v,\tau))} - \frac{6v^{3-\xi_2(v,\tau)}}{\Gamma(4-\xi_2(v,\tau))}\right)\tau$ . Exact solution:  $\mathcal{W}(v, \tau) = v^2(1-v)\tau$ . The numerical approximation, exact solution and errors between exact solution and numerical approximation are shown in Table 3, while the maximum absolute errors are shown in Table 4 at different time and space intervals along with convergence rate. The results are also shown in Figures 4–6. The 3D surface plot is constructed on  $\delta\nu = \delta\tau = 0.001$ , while plot3 is constructed on  $\delta\nu = \delta\tau = 0.1$  as shown in Figure 4. In Figure 5, the error plots are shown for  $N = 100, 500, 1000$  and  $\delta\tau = 0.001$  at  $\tau = 1$  on 3D surface, while Figure 6 shows the convergence rates w.r.t. space and time.

**Example 4.3.** Let us take  $\zeta(v, \tau) = 0.55 - 0.25e^{-v\tau}$ ,  $\xi_1(v, \tau) = 1.55 + 0.35 \cos(3\pi v\tau)$ ,  $\xi_2(v, \tau) = 0.65 + 0.25 \sin(3\pi v\tau)$ ,  $r_1 = r_2 = r_3 = 1$  and  $r_4 = -1$ .  $w(v, 0) = 0$  is the initial condition while  $w(0, \tau) = 0 = w(L, \tau)$  is the boundary condition.  $R(v, \tau) = \mathcal{R}_1(v, \tau) - \tau\mathcal{R}_2(v, \tau)$ , where  $\mathcal{R}_1(v, \tau) = \left(1 + \frac{\tau^{1-\zeta(v,\tau)}}{\Gamma(2-\zeta(v,\tau))}\right)\sin(2\pi v)$ ,  $\mathcal{R}_2(v, \tau) = \sin(2\pi v + \pi^2\xi_1(v, \tau)) - \sin(2\pi v + \pi^2\xi_2(v, \tau))$ . The exact solution is  $\mathcal{W}(v, \tau) = \tau \sin(2\pi v)$ . All results are shown in Tables 5, 6 and Figures 7–9.

**Table 1.** Absolute errors between exact and approximate solutions of Example 4.1.

$\theta = 0.5, \delta\nu = 0.01, \delta\tau = 0.01, \tau = 1$			
$\nu$	$\mathcal{W}$	$w_{approx.}$	$\ L\ $
0	0	0.000000000000415	0.000000000000415
0.1	0.108900000000000	0.108874486938645	0.000025513061355
0.2	0.193600000000000	0.193638457799857	0.000038457799857
0.3	0.254100000000000	0.254174538846443	0.000074538846443
0.4	0.290400000000000	0.290497098595359	0.000097098595359
0.5	0.302500000000000	0.302610227369723	0.000110227369723
0.6	0.290400000000000	0.290515689696830	0.000115689696830
0.7	0.254100000000000	0.254214422815980	0.000114422815980
0.8	0.193600000000000	0.193706992369054	0.000106992369054
0.9	0.108900000000000	0.108993770701635	0.000093770701635
1	0	0.0000000000007030	0.0000000000007030
$\theta = 1, \delta\nu = 0.01, \delta\tau = 0.01, \tau = 1$			
$\nu$	$\mathcal{W}$	$w_{approx.}$	$\ L\ $
0	0	0.000000000000321	0.000000000000321
0.1	0.108900000000000	0.108876698600746	0.000023301399254
0.2	0.193600000000000	0.193635404625688	0.000035404625687
0.3	0.254100000000000	0.254168526166297	0.000068526166297
0.4	0.290400000000000	0.290489234279579	0.000089234279579
0.5	0.302500000000000	0.302601278404606	0.000101278404606
0.6	0.290400000000000	0.290506276014470	0.000106276014470
0.7	0.254100000000000	0.254205086239745	0.000105086239745
0.8	0.193600000000000	0.193698227582199	0.000098227582200
0.9	0.108900000000000	0.108986041356451	0.000086041356451
1	0	0.0000000000005442	0.0000000000005442

**Table 2.** Numerical results of Example 4.1.

		$\ L\ _\infty$			Convergence					
		$\delta\tau = 0.1$	$\delta\tau = 0.01$	$\delta\tau = 0.001$	$\delta\nu_i$	$\ L\ _\infty$	order	$\delta\tau_i$	$\ L\ _\infty$	order
$\theta = 0.5$	$N = 50$	$8.6648e^{-3}$	$6.6825e^{-3}$	$9.5234e^{-4}$	$\frac{1}{50}$	$9.5234e^{-4}$	—	0.1	$2.4704e^{-5}$	—
	$N = 100$	$4.6451e^{-4}$	$4.0639e^{-4}$	$9.9494e^{-5}$	$\frac{1}{100}$	$9.9494e^{-5}$	1.3796	0.01	$2.1616e^{-5}$	0.0580
	$N = 500$	$9.7890e^{-5}$	$8.5652e^{-5}$	$4.6397e^{-5}$	$\frac{1}{500}$	$4.6397e^{-5}$	0.4740	0.005	$8.6636e^{-6}$	-0.5602
	$N = 1000$	$2.4704e^{-5}$	$2.1616e^{-5}$	$3.2626e^{-6}$	$\frac{1}{1000}$	$3.2626e^{-6}$	1.9507	0.001	$3.2626e^{-6}$	0.6068
$\theta = 1$	$N = 50$	$7.4450e^{-3}$	$4.4255e^{-3}$	$7.4450e^{-4}$	$\frac{1}{50}$	$7.4450e^{-4}$	—	0.1	$8.2645e^{-6}$	—
	$N = 100$	$4.2574e^{-4}$	$3.5875e^{-4}$	$8.5517e^{-5}$	$\frac{1}{100}$	$8.5517e^{-5}$	1.2428	0.01	$1.9091e^{-6}$	0.6364
	$N = 500$	$4.5149e^{-5}$	$3.8062e^{-5}$	$9.7387e^{-6}$	$\frac{1}{500}$	$9.7387e^{-6}$	0.5406	0.005	$1.2633e^{-6}$	0.5957
	$N = 1000$	$8.2645e^{-6}$	$1.9091e^{-6}$	$1.0752e^{-6}$	$\frac{1}{1000}$	$1.0752e^{-6}$	3.1791	0.001	$1.0752e^{-6}$	0.1002

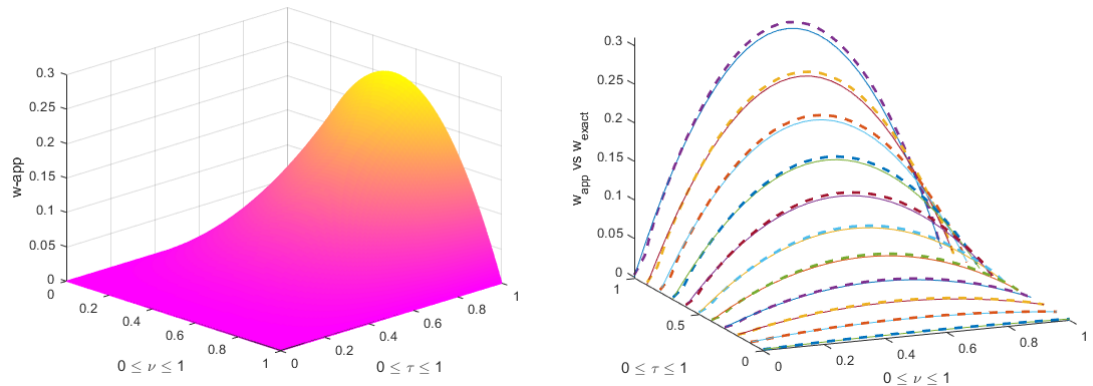


**Figure 1.** Numerical approximation for Example 4.1.

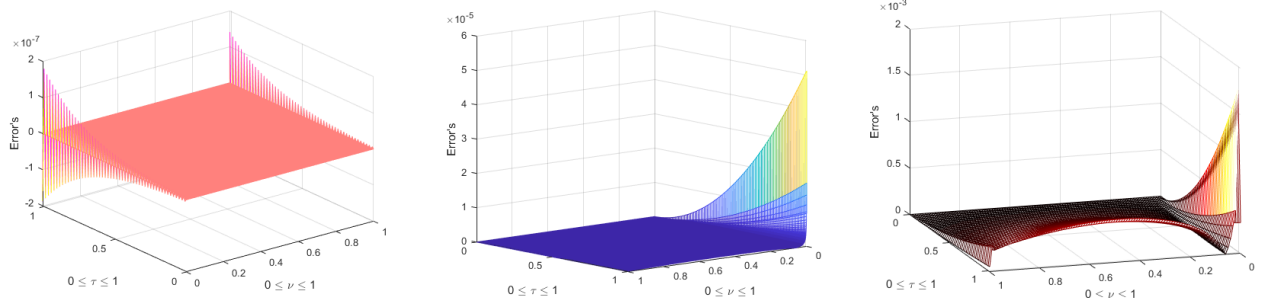


**Figure 2.** Numerical error for Example 4.1,  $N = 1000$  (left),  $N = 500$  (center),  $N = 50$  (right).

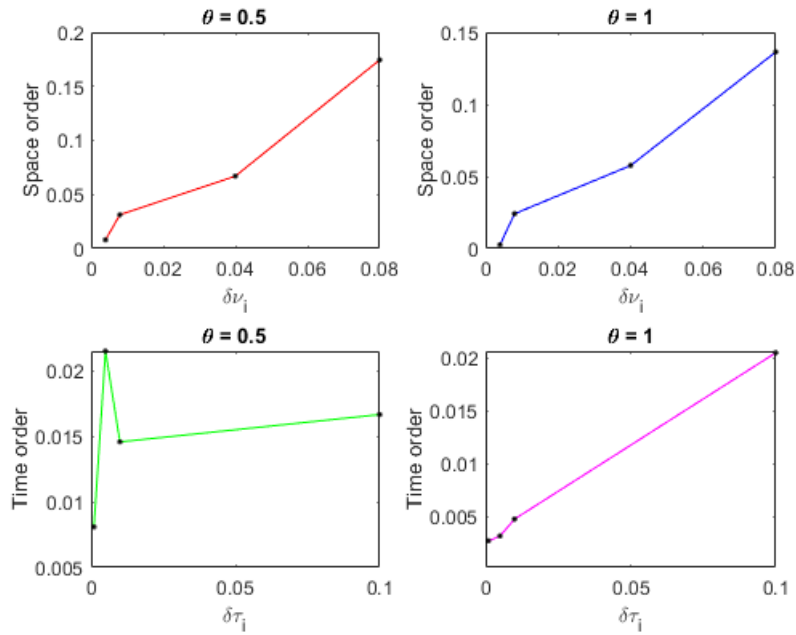


**Figure 3.** Time and Space convergence graphs for Example 4.1.

**Table 3.** Absolute errors between exact and approximate solutions of Example 4.2.

$\theta = 0.5, \delta\nu = 0.01, \delta\tau = 0.01, \tau = 1$				
$\nu$	$\mathcal{W}$	$w_{approx.}$	$\ L\ $	
0	0	0	0	
0.1	0.0099000000000000	0.009897086666315	0.000002913333685	
0.2	0.0352000000000000	0.035198375282382	0.000001624717618	
0.3	0.0693000000000000	0.069300025003365	0.000000025003365	
0.4	0.1056000000000000	0.105601780133889	0.000001780133889	
0.5	0.1375000000000000	0.137503500551076	0.000003500551076	
0.6	0.1584000000000000	0.158405082491059	0.000005082491059	
0.7	0.1617000000000000	0.161706438415009	0.000006438415009	
0.8	0.1408000000000000	0.140807489496559	0.000007489496559	
0.9	0.0891000000000000	0.089108162169441	0.000008162169441	
1	0	0	0	
$\theta = 1, \delta\nu = 0.01, \delta\tau = 0.01, \tau = 1$				
$\nu$	$\mathcal{W}$	$w_{approx.}$	$\ L\ $	
0	0	0	0	
0.1	0.0099000000000000	0.009897305273084	0.000002694726916	
0.2	0.0352000000000000	0.035198424184953	0.000001575815047	
0.3	0.0693000000000000	0.069299852438873	0.000000147561127	
0.4	0.1056000000000000	0.105601371899563	0.000001371899563	
0.5	0.1375000000000000	0.137502870365957	0.000002870365957	
0.6	0.1584000000000000	0.158404268963810	0.000004268963810	
0.7	0.1617000000000000	0.161705503690809	0.000005503690809	
0.8	0.1408000000000000	0.140806518530524	0.000006518530524	
0.9	0.0891000000000000	0.089107262287949	0.000007262287949	
1	0	0	0	

**Table 4.** Numerical results of Example 4.2.

	$\ L\ _\infty$			Convergence						
	$\delta\tau = 0.1$	$\delta\tau = 0.01$	$\delta\tau = 0.001$	$\delta\nu_i$	$\ L\ _\infty$	order	$\delta\tau_i$	$\ L\ _\infty$	order	
$\theta = 0.5$	$N = 50$	$5.9983e^{-4}$	$1.8694e^{-4}$	$1.6494e^{-4}$	$\frac{1}{50}$	$1.6494e^{-4}$	—	$0.1$	$3.0178e^{-6}$	—
	$N = 100$	$1.8809e^{-4}$	$5.4232e^{-5}$	$4.6555e^{-5}$	$\frac{1}{100}$	$4.6555e^{-5}$	-0.0543	$0.01$	$8.6729e^{-7}$	-0.0242
	$N = 500$	$3.6432e^{-5}$	$3.1094e^{-5}$	$8.9269e^{-6}$	$\frac{1}{500}$	$8.9269e^{-6}$	0.2168	$0.005$	$5.8049e^{-7}$	0.5792
	$N = 1000$	$3.0178e^{-6}$	$8.6729e^{-7}$	$2.4916e^{-7}$	$\frac{1}{1000}$	$2.4916e^{-7}$	3.2838	$0.001$	$2.4916e^{-7}$	1.0287
$\theta = 1$	$N = 50$	$8.7240e^{-4}$	$5.8862e^{-4}$	$1.7187e^{-4}$	$\frac{1}{50}$	$1.7187e^{-4}$	—	$0.1$	$8.2645e^{-6}$	—
	$N = 100$	$5.3797e^{-4}$	$4.5481e^{-5}$	$3.0639e^{-5}$	$\frac{1}{100}$	$3.0639e^{-5}$	0.6086	$0.01$	$7.9495e^{-7}$	0.5874
	$N = 500$	$3.3366e^{-5}$	$1.4355e^{-5}$	$8.8284e^{-6}$	$\frac{1}{500}$	$8.8284e^{-6}$	-0.0362	$0.005$	$1.8515e^{-7}$	1.6496
	$N = 1000$	$8.9157e^{-6}$	$7.9495e^{-7}$	$1.1085e^{-7}$	$\frac{1}{1000}$	$1.1085e^{-7}$	3.2678	$0.001$	$1.1085e^{-7}$	0.3187

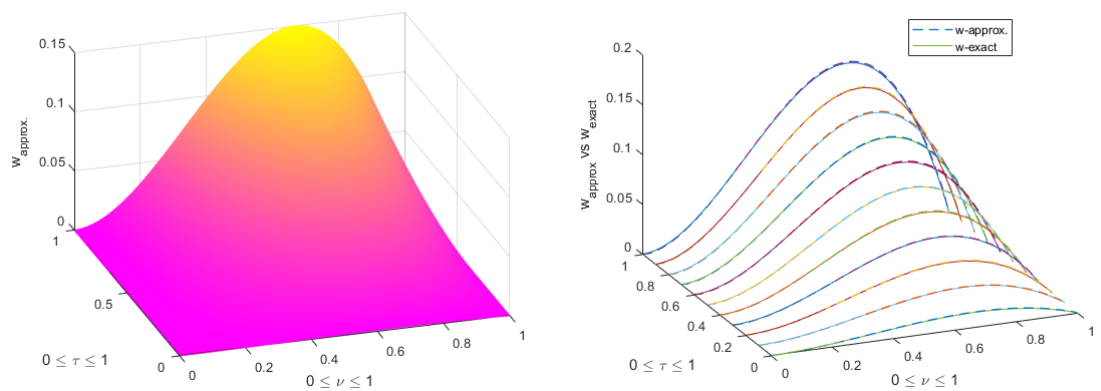


**Figure 4.** Numerical approximation for Example 4.2.

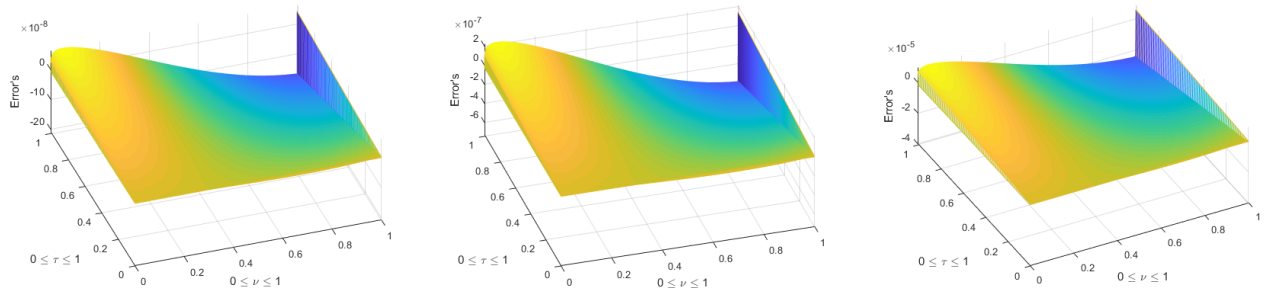


**Figure 5.** Numerical error for Example 4.2,  $N = 1000$  (left),  $N = 500$  (center),  $N = 100$  (right).

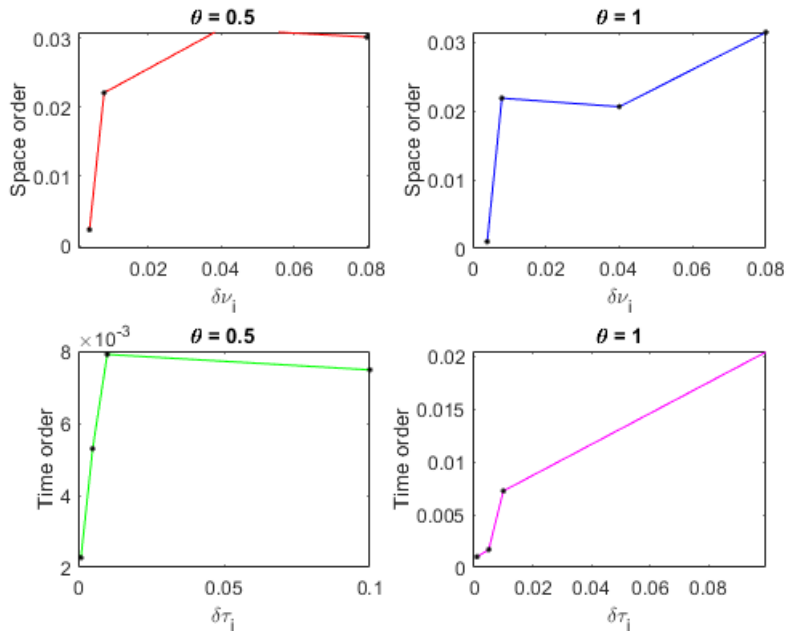


**Figure 6.** Time and Space convergence graphs for Example 4.2.

**Table 5.** Absolute errors between exact and approximate solutions of Example 4.3.

$\theta = 0.5, \delta\nu = 0.01, \delta\tau = 0.01, \tau = 1$				
$\nu$	$\mathcal{W}$	$w_{approx.}$	$\ L\ $	
0	0	0	0	0
0.1	0.646563777521720	0.646563976092694	0.000000198570974	
0.2	1.046162167924669	1.046162715575450	0.000000547650781	
0.3	1.046162167924669	1.046162855471273	0.000000687546604	
0.4	0.646563777521721	0.646564342344714	0.000000564822993	
0.5	0.000000000000000	0.000000000000000	0.000000000000000	
0.6	-0.646563777521720	-0.646563976092694	0.000000198570974	
0.7	-1.046162167924669	-1.046162715575450	0.000000547650781	
0.8	-1.046162167924669	-1.046162855471273	0.000000687546604	
0.9	-0.646563777521721	-0.646564342344714	0.000000564822993	
1	0	0	0	0
$\theta = 1, \delta\nu = 0.01, \delta\tau = 0.01, \tau = 1$				
$\nu$	$\mathcal{W}$	$w_{approx.}$	$\ L\ $	
0	0	0	0	0
0.1	0.646563777521720	0.646563885272363	0.000000107750643	
0.2	1.046162167924669	1.046162549758231	0.000000381833562	
0.3	1.046162167924669	1.046162677993707	0.000000510069038	
0.4	0.646563777521721	0.646564220997199	0.000000443475479	
0.5	0.000000000000000	0.000000000000000	0.000000000000000	
0.6	-0.646563777521720	-0.646563885272363	0.000000107750643	
0.7	-1.046162167924669	-1.046162549758231	0.000000381833562	
0.8	-1.046162167924669	-1.046162677993707	0.000000510069038	
0.9	-0.646563777521721	-0.646564220997200	0.000000443475479	
1	0	0	0	0

**Table 6.** Numerical results of Example 4.3.

	$\ L\ _\infty$			Convergence						
	$\delta\tau = 0.1$	$\delta\tau = 0.01$	$\delta\tau = 0.001$	$\delta\nu_i$	$\ L\ _\infty$	order	$\delta\tau_i$	$\ L\ _\infty$	order	
$\theta = 0.5$	$N = 50$	$7.5449e^{-4}$	$4.4194e^{-4}$	$1.4712e^{-4}$	$\frac{1}{50}$	$1.4712e^{-4}$	—	$0.1$	$6.8770e^{-7}$	—
	$N = 100$	$1.2950e^{-4}$	$9.8713e^{-5}$	$9.0805e^{-5}$	$\frac{1}{100}$	$9.0805e^{-5}$	-0.0543	$0.01$	$1.7226e^{-7}$	-0.0242
	$N = 500$	$1.5349e^{-5}$	$6.3320e^{-6}$	$1.2727e^{-6}$	$\frac{1}{500}$	$1.2727e^{-6}$	0.2168	$0.005$	$1.1029e^{-7}$	0.5792
	$N = 1000$	$6.8770e^{-7}$	$1.7226e^{-7}$	$4.3104e^{-8}$	$\frac{1}{1000}$	$4.3104e^{-8}$	3.2838	$0.001$	$4.3104e^{-8}$	1.0287
$\theta = 1$	$N = 50$	$1.8739e^{-4}$	$7.7443e^{-5}$	$7.4214e^{-5}$	$\frac{1}{50}$	$7.4214e^{-5}$	—	$0.1$	$5.1276e^{-7}$	—
	$N = 100$	$4.8074e^{-5}$	$1.2848e^{-5}$	$8.0955e^{-6}$	$\frac{1}{100}$	$8.0955e^{-6}$	0.6086	$0.01$	$1.2845e^{-7}$	0.5874
	$N = 500$	$8.2614e^{-6}$	$2.0842e^{-6}$	$8.0035e^{-7}$	$\frac{1}{500}$	$8.0035e^{-7}$	-0.0362	$0.005$	$3.2142e^{-8}$	1.6496
	$N = 1000$	$5.1276e^{-7}$	$1.2845e^{-7}$	$2.0574e^{-8}$	$\frac{1}{1000}$	$2.0574e^{-8}$	3.2678	$0.001$	$2.0574e^{-8}$	0.3187

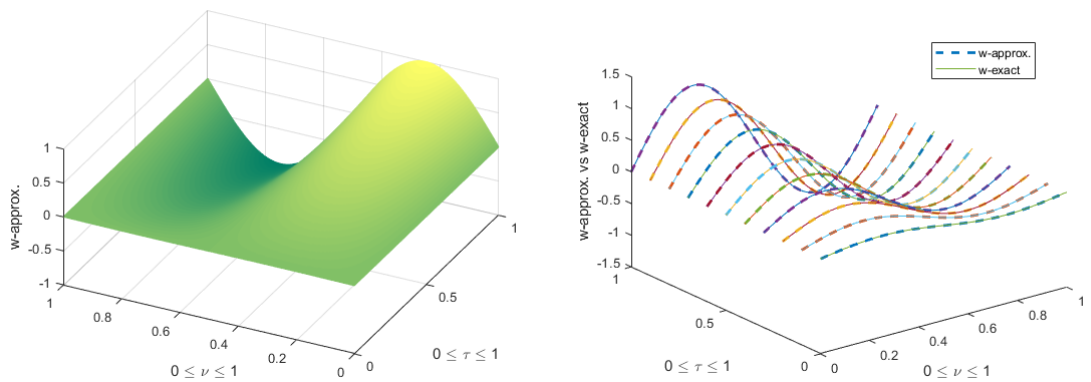


**Figure 7.** Numerical approximation for Example 5.3.

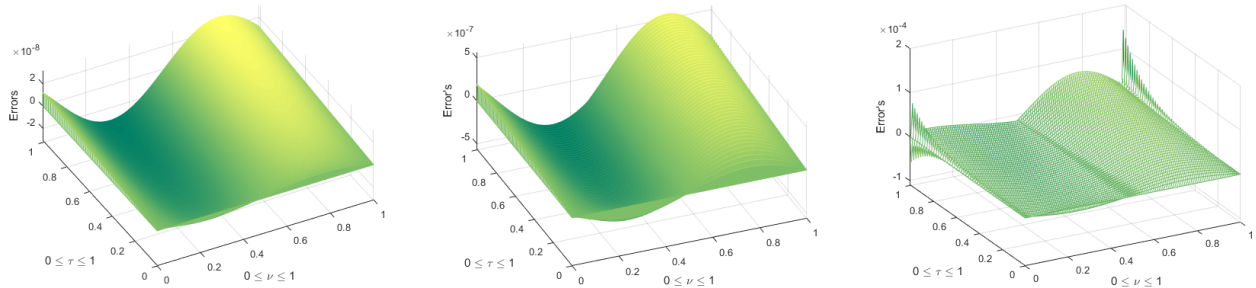


**Figure 8.** Numerical error for Example 4.3,  $N = 1000$  (left),  $N = 500$  (center),  $N = 50$  (right).

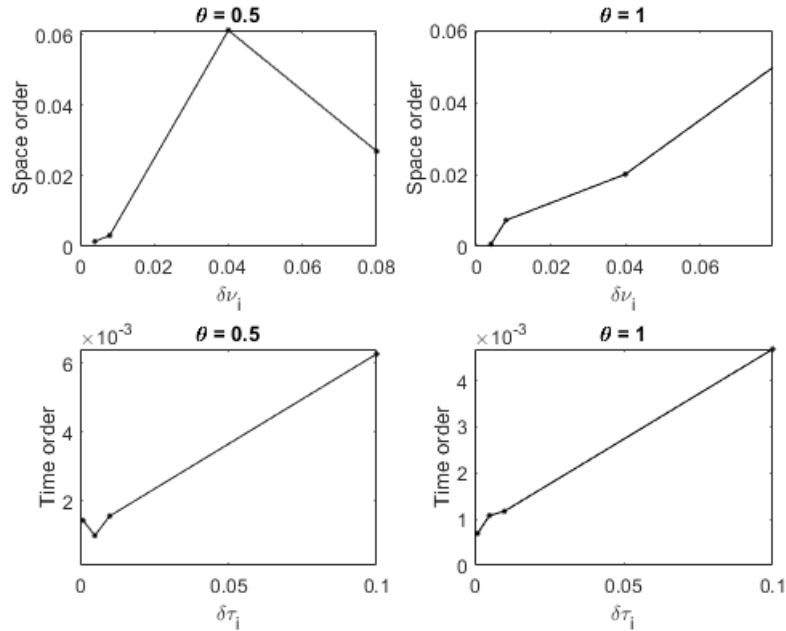


**Figure 9.** Time and Space convergence graphs for Example 4.3.

Table 7 represents the  $\|L\|_\infty$  at  $N = 50, 100, 500, 1000$  and  $\delta\tau = 0.001$  vs CPU machine time. These results are computed by MATLAB 2018b software while the hardware machine is HP core i7, 11th generation processor, 16GB RAM, 2GB GPU.

**Table 7.** Numerical results vs machine time of all examples  $\delta\tau = 0.001$ .

Example 4.1			Example 4.2			Example 4.3		
N	$\ L\ _\infty$	Machine time (sec)						
50	$9.5234e^{-4}$	12	$1.6494e^{-4}$	11.205	$1.4712e^{-4}$	11.5		
100	$9.9494e^{-5}$	19	$4.6555e^{-5}$	18	$9.0805e^{-5}$	21.223		
500	$4.6397e^{-5}$	265	$8.9269e^{-6}$	254	$1.2727e^{-6}$	291		
1000	$3.2626e^{-6}$	1184	$2.4916e^{-7}$	1126	$4.3104e^{-8}$	1201		

## 5. Conclusions

Meshfree RBF method based on the Gaussian function is used for the numerical solution of the time-space dependent order advection-dispersion mobile-immobile equation. Time derivatives are dealt with by Caputo derivative operator, while space derivatives are dealt with by Riesz, Grünwald-Letnikov derivative operators. The stability and convergence of the method are discussed and the efficiency is analyzed by the maximum norm. The method is tested through some examples and the results are shown in tables and figures. In the future, based on these results, it will be more interesting to see how the proposed method can work on such PDE models defined on irregular domains, complex function orders, and in case when the exact solution of the PDE model is unknown.

## Conflict of interest

The authors have no conflicts of interest.

## Acknowledgments

The work was supported by Princess Nourah bint Abdulrahman University Researchers Supporting Project number (PNURSP2023R8), Princess Nourah bint Abdulrahman University, Riyadh, Saudi Arabia.

## References

1. M. M. Meerschaert, D. A. Benson, B. Bäumer, Multidimensional advection and fractional dispersion, *Phys. Rev. E*, **59** (1999), 5026. <https://doi.org/10.1103/physreve.59.5026>
2. J. Bear, *Dynamics of fluids in porous media*, New York: American Elsevier Publishing Company, 1972.
3. R. Schumer, D. A. Benson, M. M. Meerschaert, B. Baeumer, Fractal mobile/immobile solute transport, *Water Resour. Res.*, **39** (2003), 1296. <https://doi.org/10.1029/2003WR002141>
4. K. H. Coats, B. D. Smith, Dead-end pore volume and dispersion in porous media, *SPE J.*, **4** (1964), 73–84. <https://doi.org/10.2118/647-PA>

5. F. Bauget, M. Fourar, Non-fickian dispersion in a single fracture, *J. Contam. Hydrol.*, **100** (2008), 137–148. <https://doi.org/10.1016/j.jconhyd.2008.06.005>
6. B. Berkowitz, Charaterizing flow and transport in fractured geological media: a review, *Adv. Water Resour.*, **25** (2002), 861–884. [https://doi.org/10.1016/S0309-1708\(02\)00042-8](https://doi.org/10.1016/S0309-1708(02)00042-8)
7. H. Scher, M. Lax, Stochastic transport in a disordered solid. I. theory, *Phys. Rev. B*, **7** (1973), 4491. <https://doi.org/10.1103/PhysRevB.7.4491>
8. I. Podulbny, *Fractional differential equations*, Academic Press, 1998.
9. K. S. Miller, B. Ross, *An introduction to the fractional calculus and fractional differential equations*, New York: Wiley, 1993.
10. D. Baleanu, J. A. T. Machado, A. C. J. Luo, *Fractional dynamics and control*, New York: Springer, 2012. <https://doi.org/10.1007/978-1-4614-0457-6>
11. V. E. Tarasov, *Fractional dynamics: applications of fractional calculus to dynamics of particles, fields and media*, Berlin, Heidelberg: Springer, 2010.
12. R. Hilfer, *Applications of fractional calculus in physics*, Singapore: World Scientific, 2000. <https://doi.org/10.1142/3779>
13. M. A. Abdelkawy, M. A. Zaky, A. H. Bhrawy, D. Baleanu, Numerical simulation of time variable fractional order mobile-immobile advection-dispersion model, *Rom. Rep. Phys.*, **67** (2015), 773–791.
14. B. Y. Wang, J. Y. Zhang, G. W. Yan, Numerical simulation of the fractional dispersion advection equations based on the lattice Boltzmann model, *Math. Probl. Eng.*, **2020** (2020), 2570252. <https://doi.org/10.1155/2020/2570252>
15. I. I. Goria, A reliable algorithm for multi-dimensional mobile/immobile advection-dispersion equation with variable order fractional, *Indian J. Sci. Technol.*, **11** (2018), 1–9. <https://doi.org/10.17485/ijst/2018/v11i30/127486>
16. B. Yu, X. Y. Jiang, H. T. Qi, Numerical method for the estimation of the fractional parameters in the fractional mobile/immobile advection-diffusion model, *Int. J. Comput. Math.*, **95** (2018), 1131–1150. <https://doi.org/10.1080/00207160.2017.1378811>
17. H. Pourbashash, D. Baleanu, M. M. A. Qurashi, On solving fractional mobile/immobile equation, *Adv. Mech. Eng.*, **9** (2017), 1–12.
18. P. D. Lax, R. D. Richtmyer, Survey of the stability of linear finite difference equations, *Commun. Pure Appl. Math.*, **9** (1956), 267–293. <https://doi.org/10.1002/cpa.3160090206>
19. O. Nikan, Z. Avazzadeh, J. A. T. Machado, Numerical approach for modeling fractional heat conduction in porous medium with the generalized Cattaneo model, *Appl. Math. Model.*, **100** (2021), 107–124. <https://doi.org/10.1016/j.apm.2021.07.025>
20. O. Nikan, Z. Avazzadeh, Numerical simulation of fractional evolution model arising in viscoelastic mechanics, *Appl. Numer. Math.*, **169** (2021), 303–320. <https://doi.org/10.1016/j.apnum.2021.07.008>
21. X. T. Liu, H. G. Sun, Y. Zhang, Z. J. Fu, A scale-dependent finite difference approximation for time fractional differential equation, *Comput. Mech.*, **63** (2019), 429–442. <https://doi.org/10.1007/s00466-018-1601-x>

22. Z. C. Tang, Z. J. Fu, H. G. Sun, X. T. Liu, An efficient localized collocation solver for anomalous diffusion on surfaces, *Fract. Calc. Appl. Anal.*, **24** (2021), 865–894. <https://doi.org/10.1515/fca-2021-0037>
23. Z. J. Fu, L. W. Yang, Q. Xi, C. S. Liu, A boundary collocation method for anomalous heat conduction analysis in functionally graded materials, *Comput. Math. Appl.*, **88** (2021), 91–109. <https://doi.org/10.1016/j.camwa.2020.02.023>
24. H. Xu, S. J. Liao, X. C. You, Analysis of nonlinear fractional partial differential equations with the homotopy analysis method, *Commun. Nonlinear Sci. Numer. Simul.*, **14** (2009), 1152–1156. <https://doi.org/10.1016/j.cnsns.2008.04.008>
25. A. A. Ragab, K. M. Hemida, M. S. Mohamed, M. A. A. E. Salam, Solution of time-fractional Navier-Stokes equation by using homotopy analysis method, *Gen. Math. Notes*, **13** (2012), 13–21.
26. S. Chen, F. Liu, P. Zhuang, V. Anh, Finite difference approximations for the fractional Fokker-Planck equation, *Appl. Math. Model.*, **33** (2009), 256–273. <https://doi.org/10.1016/j.apm.2007.11.005>
27. Y. M. Lin, C. J. Xu, Finite difference/spectral approximations for the time-fractional diffusion equation, *J. Comput. Phys.*, **225** (2007), 1533–1552. <https://doi.org/10.1016/j.jcp.2007.02.001>
28. C. P. Li, Y. H. Wang, Numerical algorithm based on adomian decomposition for fractional differential equations, *Comput. Math. Appl.*, **57** (2009), 1672–1681. <https://doi.org/10.1016/j.camwa.2009.03.079>
29. H. Fatoorehchi, R. Rach, H. Sakhaeinia, Explicit Frost-Kalkwarf type equations for calculation of vapour pressure of liquids from triple to critical point by the adomian decomposition method, *Can. J. Chem. Eng.*, **95** (2017), 2199–2208. <https://doi.org/10.1002/cjce.22853>
30. A. Samad, J. Muhammad, Meshfree collocation method for higher order KdV equations, *J. Appl. Comput. Mech.*, **7** (2021), 422–431. <https://doi.org/10.22055/JACM.2020.34874.2493>
31. P. Thounthong, M. N. Khan, I. Hussain, I. Ahmad, P. Kumam, Symmetric radial basis function method for simulation of elliptic partial differential equations, *Mathematics*, **6** (2018), 327. <https://doi.org/10.3390/math6120327>
32. G. E. Fasshauer, *Meshfree approximation methods with Matlab*, Word Scientific, 2007. <https://doi.org/10.1142/6437>
33. V. R. Hosseini, W. Chen, Z. Avazzadeh, Numerical solution of fractional telegraph equation by using radial basis functions, *Eng. Anal. Bound. Elem.*, **38** (2014), 31–39. <https://doi.org/10.1016/j.enganabound.2013.10.009>
34. A. Samad, I. Siddique, F. Jarad, Meshfree numerical integration for some challenging multi-term fractional order PDEs, *AIMS Math.*, **7** (2022), 14249–14269. <https://doi.org/10.3934/math.2022785>
35. F. Z. Wang, K. H. Zheng, I. Ahmad, H. Ahmad, Gaussian radial basis functions method for linear and nonlinear convection-diffusion models in physical phenomena, *Open Phys.*, **19** (2021), 69–76. <https://doi.org/10.1515/phys-2021-0011>

36. F. Z. Wang, I. Ahmad, H. Ahmad, M. D. Alsulami, K. S. Alimgeer, C. Cesarano, et al., Meshless method based on RBFs for solving three-dimensional multi-term time fractional PDEs arising in engineering phenomenons, *J. King Saud Univ. Sci.*, **33** (2021), 101604. <https://doi.org/10.1016/j.jksus.2021.101604>
37. M. N. Khan, I. Ahmad, H. Ahmad, A radial basis function collocation method for space-dependent inverse heat problems, *J. Appl. Comput. Mech.*, **6** (2020), 1187–1199.
38. A. Ali, S. Islam, S. Haq, A computational meshfree technique for the numerical solution of the two dimensional coupled Burgers' equations, *Int. J. Comput. Methods Eng. Sci. Mech.*, **10** (2009), 406–422. <https://doi.org/10.1080/15502280903108016>
39. C. F. M. Coimbra, Mechanica with variable-order differential operators, *Ann. Phys.*, **12** (2003), 692–703.
40. H. Jiang, F. Liu, I. Turner, K. Burrage, Analytical solutions for the multi-term time-space Caputo-Riesz fractional advection-diffusion equations on a finite domain, *J. Math. Anal. Appl.*, **389** (2012), 1117–1127. <https://doi.org/10.1016/j.jmaa.2011.12.055>



AIMS Press

© 2023 the Author(s), licensee AIMS Press. This is an open access article distributed under the terms of the Creative Commons Attribution License (<http://creativecommons.org/licenses/by/4.0/>)